# Dynamic Model for Subcritical Combining Flows in Channel Junctions

Shazy Shabayek[1]; Peter Steffler, A.M.ASCE[2]; and Faye Hicks, M.ASCE[3]

**Abstract:** A one-dimensional theoretical model for subcritical flows in combining open channel junctions is developed. Typical examples of these junctions are encountered in urban water treatment plants, irrigation and drainage canals, and natural river systems. The model is based on applying the momentum principle in the streamwise direction to two control volumes in the junction together with overall mass conservation. Given the inflow discharges and the downstream depth, the proposed model solves for each of the upstream depths. The interfacial shear force between the two control volumes, the boundary friction force, and the separation zone shear force downstream of the lateral channel entrance are included. Predictions based on the proposed approach are shown to compare favorably with existing experimental data, previous theories, and conventional junction modeling approaches. The main advantages of the proposed model are that the proposed model does not assume equal upstream depths and that the dynamic treatment of the junction flow is consistent with that of the channel reaches in a network model.

**DOI:** 10.1061/(ASCE)0733-9429(2002)128:9(821)

**CE Database keywords:** Dynamic models; Open channel flow; Shear forces; Flow separation.

## Introduction

Open channel networks are often encountered in water resources engineering. Typical examples include conveyance structures in urban water treatment plants, irrigation and drainage canals, and natural river systems. In addition to the external boundary conditions for the whole network and the interior conservation equations for each computational channel segment, a set of compatibility relationships or interior boundary conditions are also required for each junction.

Currently, most numerical models of open channel networks provide the required equations by applying mass and energy conservation principles at the junctions. Since energy losses and differences in velocity heads are difficult to evaluate, the interior boundary conditions may simply diminish to the equality of water surface elevations and the continuity of discharge, as in the One-Dimensional Hydrodynamic Model (Environment Canada 1988); Mike 11 model (Danish Hydraulic Institute 1999); and Chaudhry (1993). Thus, physical effects considered significant enough to be included in the channel reaches of these network models are neglected when handling the junctions. Further, equality of the water surface elevations may be unrealistic for dynamic unsteady flow applications such as ice jam surges or dam break floods in tributary channels as well as abrupt gate closure in irrigation networks.

Previous studies on combining open channel flows Taylor 1944; Webber and Greated 1966; and Gurram 1994 proposed theoretical approaches, based on conservation of mass and momentum, to solve for the upstream-to-downstream depth ratio. Boundary friction effects were neglected and equality of the upstream depths was assumed. Hsu et al. (1998) applied overall mass and energy conservation to the junction and momentum conservation to two control volumes in the junction and computed an energy loss coefficient as well as the depth ratio. All of these studies were for equal-width junction flows.

The purpose of this study is to provide a framework that leads to an improved set of internal boundary conditions, consistent with the level of approximation embodied in the St. Venant equations. A one-dimensional theoretical model for the case of steady subcritical combining open channel junction flows which can be incorporated as an enhancement in current open channel network models is introduced. The proposed model is based on applying the momentum principle together with mass continuity through the junction. As illustrated in Fig. 1, two control volumes are considered: one for the main channel flow, and the other for the lateral channel flow. The control volumes are bounded by streamlines such that there are no lateral mass fluxes. Conservation of longitudinal momentum is applied to each control volume in the respective streamwise directions. The interfacial shear force between the two control volumes, the separation zone shear force acting on the lateral channel control volume, the weight component in the direction of the slope, and the boundary friction force are accounted for in the analysis. Two shear coefficients are introduced to evaluate the interfacial and separation shear forces that occur on the lateral boundaries of the control volumes. The velocities and water surface elevations are assumed to be constant across the channels at the inflow and outflow sections of the control volumes. Channel widths, control volume lengths, resistance characteristics, and slopes are assumed to be known. Given the upstream discharges and the downstream depth, the proposed

[1]Graduate Student, Dept. of Civil and Environmental Engineering, Univ. of Alberta, Edmonton AB, Canada T6G 2G7.

[2]Professor, Dept. of Civil and Environmental Engineering, Univ. of Alberta, Edmonton AB, Canada T6G 2G7.

[3]Professor, Dept. of Civil and Environmental Engineering, Univ. of Alberta, Edmonton AB, Canada T6G 2G7.

Note. Discussion open until February 1, 2003. Separate discussions must be submitted for individual papers. To extend the closing date by one month, a written request must be filed with the ASCE Managing Editor. The manuscript for this paper was submitted for review and possible publication on December 28, 1998; approved on February 5, 2002. This paper is part of the ***Journal of Hydraulic Engineering***, Vol. 128, No. 9, September 1, 2002. ©ASCE, ISSN 0733-9429/2002/9-821–828/$8.00+$.50 per page.

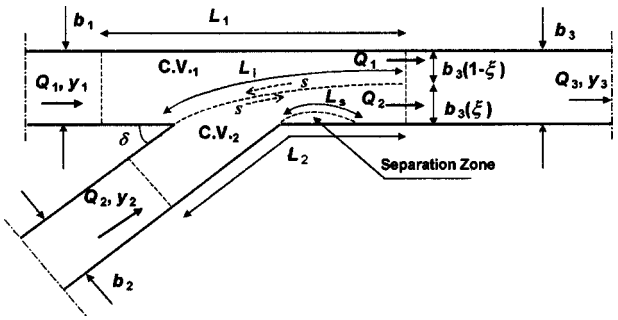


**Fig. 1.** Open channel junction with control volumes and notation

model solves for each of the upstream depths. The two empirical coefficients should be calibrated at a specific site, with guidance from experimental values. Including the weight and the boundary friction force allows the model to be scaled up to prototype scale applications and makes the handling of the junctions consistent with that of the channel reaches.

The two-control volume approach chosen for this model is distinct from previous theories in that it does not assume equality of the upstream depths. Clearly, this assumption leads to a simpler analysis and is well justified for existing experiments in steady subcritical combining flows. However, our aim is to develop a methodology with a much broader range of application, including dividing flows and eventually surge propagation through channel junctions. In these cases, an equal depth approximation is tantamount to neglecting the junction dynamics entirely (Garcia-Navarro and Savirón 1992). The purpose of this paper, then, is to verify the two-control volume approach for the subcritical combining steady flow case as a first step toward the development of a more general formulation.

## Available Experimental Data

The experimental observations of Taylor (1944); Webber and Greated (1966); Gurram (1994); and Hsu et al. (1998) are used for a preliminary model verification and investigation of the associated coefficients. While the intended application of the model includes large scale, high-aspect ratio canal and river junctions, these experiments are the only ones available for validation.

Fig. 1 shows the geometric configuration of the junctions considered in the studies of Taylor (1944); Webber and Greated (1966); Gurram (1994); and Hsu et al. (1998). The subscripts 1 and 3 refer to the main channel upstream and downstream sections, respectively, and the subscript 2 refers to the lateral channel upstream section. In these studies, the flow was subcritical throughout and the channels were horizontal, rectangular channels of equal width, with smooth boundaries and small aspect ratios ($b/y=1.5-6$). Fully turbulent flow, with Reynolds numbers of 3,000–74,000, was achieved for most cases. Table 1 shows the experimental details for these studies where: $b$, $y$, $Q$, $\xi$, $\delta$, R, and F are the width, depth, discharge, discharge ratio ($\xi=Q_2/Q_3$), junction angle, Reynolds number, and Froude number, respectively. Where the specified data was not explicitly provided in the published materials, the table cells were left blank. Webber and Greated (1966) and Gurram (1994) presented their results in the form of plots of the main channel depth ratio, $\eta_1=y_1/y_3$, versus the downstream Froude number, $F_3$, for the different discharge ratios, $\xi$, and the different angles, $\delta$. Taylor (1944) plotted $\eta_1$ versus a lateral channel kineticity coefficient which can be related to $F_3$ and $\xi$. Hsu et al. (1998) kept the downstream Froude number, $F_3$, approximately constant (0.59–0.62) and plotted the variation of $\eta_1$ with $\xi$. The study of Hsu et al. (1998) was the only study that presented upstream depth measurements in the lateral channel.

## Proposed Theoretical Approach

Fig. 1 shows the channel geometry to be considered in this analysis. The six variables to be evaluated are the depths and discharges at the three sections enclosing the junction. In the case of subcritical flow, the boundary conditions are specified as the two inflow discharges, $Q_1$ and $Q_2$, and a third downstream boundary condition that can be either a fixed depth or a rating curve. These boundary conditions define three of the six variables in the problem or two variables and one equation. Hence, three additional equations are required for closing the problem.

In this analysis, the junction is divided into two control volumes, as shown in Fig. 1. The channels are all assumed to be of rectangular cross section. The streamline curvature is considered small and vertical accelerations negligible; hence, the vertical pressure distribution is assumed to be hydrostatic. Uniform velocity distributions and parallel streamlines are also assumed at the inflow and outflow sections of the control volumes.

Applying overall mass conservation to the junction and conservation of streamwise momentum to each of the two control volumes provides the three necessary equations. Mass conservation gives

$$Q_1+Q_2=Q_3 \tag{1}$$

Momentum conservation is applied to each control volume in the respective streamwise direction;however, direct curvilinear flow effects are neglected as the most important apparent forces due to curvature occur in the transverse direction. Transverse variations of velocity and depth due to curvature are assumed to be small compared to the section averaged values. This level of approximation is implicit when the usual one-dimensional momentum equation is applied to curved channel reaches. Then, con-

**Table 1.** Experimental Details for Previous Studies

| Author date | Taylor (1944) | Webber and Greated (1966) | Gurram (1994) | Hsu et al. (1998) |
|---|---|---|---|---|
| $b_1$, $b_2$, $b_3$ (mm) | 101.6 | 127 | 500 | 155 |
| $y_3$ (mm) | | | 60–100 | 80–91 |
| $Q_3$ ($m^3/s$) | | | 0.037–0.125 | 0.058–0.071 |
| $\xi$ | 0.40, 0.60, 0.80 | 0.20, 0.40, 0.50, 0.60, 0.80 | 0.25, 0.50, 0.75 | 0.092–0.918 |
| $\delta$ | 45°, 135° | 30°, 60°, 90° | 30°, 60°, 90° | 30°, 45°, 60° |
| $R_3$ | | >3000 | 24,000–74,000 | 37,000–46,000 |
| $F_3$ | 0.20–0.75 | 0.20–0.60 | 0.25, 0.50, 0.75, 1.00 | 0.59–0.62 |

servation of momentum in the streamwise direction for the main channel control volume, C.V.$_1$, gives

$$-\rho Q_1 V_1 + \rho Q_1 V_3 = P_1 - P_{31} + B_1 + W_1 - S - F_{b1} \quad (2)$$

and for the lateral channel control volume, C.V.$_2$

$$-\rho Q_2 V_2 + \rho Q_2 V_3 = P_2 - P_{32} + B_2 + W_2 + S - F_{b2} - F_s \quad (3)$$

where $\rho$ = water density; $V$ = mean velocity; $P$ = hydrostatic water pressure force acting on the control surface; $B$ = pressure force component due to the change in the control volume width; $W$ = component of the weight of water in the control volume in the downslope direction; $S$ = shear force on the interface between the two control volumes; $F_b$ = friction force acting on the solid boundaries of the control volumes; and $F_s$ = shear force acting on the lateral channel control volume due to the separation zone forming downstream of the lateral channel entrance.

The hydrostatic forces $P_1$, $P_2$, $P_{31}$, and $P_{32}$ are due to the water pressure on the upstream and downstream boundaries of the two control volumes. These forces are given by

$$P = \frac{1}{2}\gamma y^2 b \quad (4)$$

where $y$ = depth of water; $\gamma$ = specific weight of water; and $b$ = width of the section under consideration.

The pressure force $B$ acts in the longitudinal direction on the lateral boundaries of each control volume. This pressure force can be approximated based on the average of the upstream depths of the two control volumes and the difference in width for each of the two control volumes to give

$$B_1 = \frac{1}{2}\gamma\left(\frac{y_1+y_2}{2}\right)^2 [b_3(1-\xi) - b_1] \quad (5)$$

for C.V.$_1$, and for C.V.$_2$

$$B_2 = \frac{1}{2}\gamma\left(\frac{y_1+y_2}{2}\right)^2 (b_3\xi - b_2) \quad (6)$$

$B_1$ and $B_2$ are not equal because, depending on the discharge ratio, the amount of contraction experienced by the two control volumes may be different. Physically, the pressure on the interface between the two control volumes is equal and opposite. However, the contribution to the longitudinal momentum balance may differ due to the differing alignments of the control volumes. In addition, pressure contributions from the side walls are considered to be lumped into this net force.

The choice of upstream depths is based on the observation that the rate of width change is greatest at the upstream point of the junction. Other formulations, based on combinations of upstream and downstream depths were tested and found to give inferior results.

$W$ is the downstream component of the weight of water in each control volume. These forces can be approximated as

$$W_1 = \gamma\left(\frac{A_1 + A_{31}}{2}\right) L_1 S_o \quad (7)$$

$$W_2 = \gamma\left(\frac{A_2 + A_{32}}{2}\right) L_2 S_o \quad (8)$$

where $A$ = average cross-sectional area of the control volume and $S_o$ = longitudinal slope of the junction. $L_1$ and $L_2$ = outer lengths of the two control volumes. The control volume lengths (and thus $L_1$ and $L_2$), should be set far enough upstream and downstream of the junction that the water surface elevation and velocity distributions can be assumed to be uniform across the respective channels. For the purpose of this paper, including comparisons with experimental data, $L_1$ and $L_2$ are set to twice the corresponding channel width.

$S$ is the shear force on the interface between C.V.$_1$ and C.V.$_2$. It acts on both control volumes, parallel to the interface, but in opposite directions in each. This force can be estimated as the average shear stress multiplied by the area of the interface. Here it is approximated as

$$S = C_f \frac{\rho(V_1^2 - V_2^2)}{2}\left(\frac{y_1+y_2}{2}\right) L_i \quad (9)$$

where $C_f$ = coefficient of friction; $V_1$ and $V_2$ = cross-sectionally averaged longitudinal velocities in the main and the lateral upstream channels, respectively, and $L_i$ = length of the interface. The interfacial shear stress has a maximum value at the upstream point where the two channels combine and the difference in velocity is largest, and tends to decrease in the downstream direction. Hence, the calculations for the shear stress and the depth of the interface are based on the incoming flow velocities, and the average of the upstream depths. The length of the interface is assumed to be proportional to the harmonic mean of the downstream widths of the two control volumes. This assumption is based on the linear lateral growth rate of plane compound shear layers (Rajaratnam 1976) and the transverse distance to the nearest side wall. Combining all constants and coefficients into a single parameter, $K^*$, allows this shear force to be written in the following form:

$$S = K^* \rho(V_1^2 - V_2^2)(y_1 + y_2)[2b_3\xi(1-\xi)] \quad (10)$$

$F_{b1}$ and $F_{b2}$ = friction forces acting on the two control volumes due to the bed and the walls of the channels. These terms should be modeled in the same way as in channel control volumes and are computed as the average shear stress multiplied by the area of the solid boundary for each control volume giving

$$F_{b1} = \rho\left(\frac{V_3}{C_*}\right)^2 [b_3(1-\xi) + y_3](L_1) \quad (11)$$

$$F_{b2} = \rho\left(\frac{V_3}{C_*}\right)^2 (b_3\xi + y_3)(L_2) \quad (12)$$

where $C_*$ = nondimensional Chezy coefficient.

$F_s$ is the separation zone shear force. It acts on the lateral channel control volume, C.V.$_2$, only, due to the recirculating flow downstream of the lateral channel entrance. It is computed in a similar way as the interfacial shear force giving

$$F_s = C_f \frac{\rho V_2^2}{2} y_2 L_s \quad (13)$$

where $C_f$ = coefficient of friction and $L_s$ = length of the separation zone interface.

In a manner analogous to the calculation of the interfacial shear force, the depth of the interface is approximated to be the lateral channel upstream depth and the length assumed to scale with the lateral channel control volume downstream width. Best and Reid (1984) found that the separation zone length also increases with the square root of the discharge ratio. This variation has been neglected in the present model for simplicity and considering that the effective shear length is considerably shorter than the total separation length. Combining all the coefficients and approximations into one coefficient, the separation zone shear coefficient, $K$, the force can be written in the form

$$F_s = K\rho V_2^2 y_2 b_3 \xi \tag{14}$$

Substituting all the above-mentioned forces into the momentum equations for the two control volumes, Eqs. (2) and (3), the resulting equation for C.V.$_1$ is

$$-\rho Q_1 V_1 + \rho Q_1 V_3 = \frac{\gamma y_1^2}{2} b_1 - \frac{\gamma y_3^2}{2} b_3 (1-\xi) + \frac{\gamma}{2}\left(\frac{y_1+y_2}{2}\right)^2 [b_3(1-\xi)-b_1] + \gamma\left(\frac{A_1+A_{31}}{2}\right) L_1 S_o$$
$$-K^*\rho(V_1^2 - V_2^2)(y_1+y_2)[2b_3\xi(1-\xi)] - \rho\left(\frac{V_3}{C_*}\right)^2 [b_3(1-\xi)+y_3](L_1) \tag{15}$$

For C.V.$_2$, this gives

$$-\rho Q_2 V_2 + \rho Q_2 V_3 = \frac{\gamma y_2^2}{2} b_2 - \frac{\gamma y_3^2}{2} b_3 \xi + \frac{\gamma}{2}\left(\frac{y_1+y_2}{2}\right)^2 (b_3\xi - b_2) + \gamma\left(\frac{A_2+A_{32}}{2}\right) L_2 S_o$$
$$+K^*\rho(V_1^2 - V_2^2)(y_1+y_2)[2b_3\xi(1-\xi)] - \rho\left(\frac{V_3}{C_*}\right)^2 [b_3\xi + y_3](L_2) - K\rho V_2^2 y_2 b_3 \xi \tag{16}$$

It should be noted that Eqs. (15) and (16) do not explicitly include the angle of the lateral channel. However, the angle may have an indirect influence through the magnitude of the separation zone shear coefficient, $K$, and the interfacial shear coefficient, $K^*$.

Nondimensionalizing Eqs. (15), and (16), using Eq. (1), in terms of the discharge ratio, $\xi = Q_2/Q_3$, the depth ratios, $\eta_1 = y_1/y_3$ and $\eta_2 = y_2/y_3$, the width ratios, $\omega_1 = b_1/b_3$ and $\omega_2 = b_2/b_3$, and the downstream Froude number, $F_3 = Q_3/(g b_3^2 y_3^3)^{0.5}$, results in the following equations:

$$\underbrace{(1-\xi) - \frac{(1-\xi)^2}{\omega_1\eta_1}}_{\text{Momentum}} = \underbrace{\frac{1}{8F_3^2}[\omega_1(3\eta_1^2 - 2\eta_1\eta_2 - \eta_2^2) + (1-\xi)(\eta_1^2 + 2\eta_1\eta_2 + \eta_2^2 - 4)]}_{\text{Net Pressure}} + \underbrace{\frac{1}{2F_3^2}\left(\frac{L_1 S_o}{y_3}\right)(\omega_1\eta_1 + (1-\xi))}_{\text{Weight}}$$
$$\underbrace{-K^*\left(\left[\frac{(1-\xi)}{\omega_1\eta_1}\right]^2 - \left[\frac{\xi}{\omega_2\eta_2}\right]^2\right)(\eta_1+\eta_2)[2\xi(1-\xi)]}_{\text{Interfacial Shear}} \underbrace{-\frac{L_1}{b_3 C_*^2}\left(1 + \frac{b_3}{y_3}(1-\xi)\right)}_{\text{Frictional Shear}} \tag{17}$$

$$\underbrace{\xi - \frac{\xi^2}{\omega_2\eta_2}}_{\text{Momentum}} = \underbrace{\frac{1}{8F_3^2}[\omega_2(3\eta_2^2 - 2\eta_1\eta_2 - \eta_1^2) + \xi(\eta_2^2 + 2\eta_1\eta_2 + \eta_1^2 - 4)]}_{\text{Net Pressure}} + \underbrace{\frac{1}{2F_3^2}\left(\frac{L_2 S_o}{y_3}\right)(\omega_2\eta_2 + \xi)}_{\text{Weight}}$$
$$\underbrace{+K^*\left(\left[\frac{(1-\xi)}{\omega_1\eta_1}\right]^2 - \left[\frac{\xi}{\omega_2\eta_2}\right]^2\right)(\eta_1+\eta_2)[2\xi(1-\xi)]}_{\text{Interfacial Shear}} \underbrace{-\frac{L_2}{b_3 C_*^2}\left(1 + \frac{b_3}{y_3}\xi\right)}_{\text{Frictional Shear}} \underbrace{-K\frac{\xi^3}{\omega_2^2\eta_2}}_{\text{Separation Shear}} \tag{18}$$

Eqs. (17) and (18) are two nonlinear equations that can be solved for the values of $\eta_1$ and $\eta_2$, given $\xi$, and $F_3$. Considering that $\xi$, $\eta_1$, $\eta_2$, $\omega_1$, and $\omega_2$ are all of the order 1, the relative order of magnitude of the various physical effects can be deduced from Eqs. (17) and (18). It can be seen that the momentum term is of order 1 and the order of magnitude of the other terms can be determined by the parameter in each term. The order of the net pressure term depends upon the value of the downstream Froude number; for cases with low values of $F_3$ the net pressure and weight terms will dominate. In the limit of $F_3 = 0$, the solution can be shown to reduce to equality of water surface elevation. The magnitude of the weight and the frictional shear terms is determined by the parameters $(LS_o/y_3)$ and $[L/(y_3 C_*^2)]$, respectively. These parameters will be significant for real-world applications where the length-to-depth ratio is large. The orders of the interfacial shear and the separation shear terms are determined by the values of $K^*$ and $K$, respectively.

## Results and Discussion

The theoretical model Eqs. (17) and (18) were solved using a Newton-Raphson procedure to calculate the depth ratios for the flow cases in the previous experimental studies. Since all these studies were performed on horizontal flumes, the weight term was not included in the analysis. A value for the nondimensional Chezy coefficient, $C_*$, was estimated for each set of experiments based on the physical model discharge and depth. $C_*$ was estimated to 17 for Taylor's (1944) and Hsu et al.'s (1998) experi-

ments and 18.5 for Gurram's (1994) experiments. Since Webber and Greated (1966) adjusted their depth measurements to remove the effect of the boundary friction, $C_*$ was set to zero for those comparisons. The lengths of the control volumes in all cases were estimated as twice the channel widths. The interfacial shear coefficient and the separation zone coefficient were calibrated using the available experimental data.

### Calibration of Interfacial Shear Coefficient, K*, and Separation Coefficient, K

For the case of equal upstream discharges, $\xi = 0.5$, and all channels of equal width, the approach velocities are very nearly equal, and thus the interfacial shear term vanishes from the equations. For the general cases where $\xi \neq 0.5$ an interfacial shear coefficient is calibrated. The measurements of Hsu et al. (1998) presented the variation of $\eta_1$ and $\eta_2$ with $\xi$ at an approximately constant value of the downstream Froude number, $F_3$. The reported range of $F_3$ of 0.59–0.62 mentioned in their study was computed including the energy correction coefficient for the main channel's downstream section. To be consistent with the present theoretical analysis, a set of downstream Froude numbers for the different runs was computed without including any correction coefficients. These values ranged between 0.52 and 0.54. Thus, an average value of $F_3 = 0.53$ was chosen to represent all of the flow cases of Hsu et al. (1998). Taylor's (1944); Webber and Greated's (1966); and Gurram's (1994) experimental data presented the variation of $\eta_1$ with $F_3$ at specific values of $\xi$. The values of $K^*$ and $K$ were calibrated for each set of experiments where the angle of intersection was held constant. The calibration for each data set was based on a least-squares error analysis between the measured and the predicted depth ratios, $\eta_1$ and $\eta_2$. Since Taylor (1944); Webber and Greated (1966); and Gurram (1994) did not provide measurements for the depth in the lateral channel and assumed the upstream depths to be equal, this assumption was employed while calibrating $K^*$ and $K$ for their data sets.

Figs. 2(a and b) present the calibrated values of the two coefficients $K^*$ and $K$ for each junction angle in each study. The figures show the variation of these calibrated coefficients with the junction angle. Fig. 2(a) shows that $K^*$ appears to decrease linearly with the junction angle if the data of Gurram (1994) is excluded. Thus, a linear trend line was plotted for this variation. The equation of this line is

$$K^* = -0.0015\delta + 0.30 \tag{19}$$

with a coefficient of determination of 0.92. Including Gurram's (1994) calibrated $K^*$ data points, the variation of $K^*$ with the junction angle may be also considered constant. Thus, a mean value of $K^* = 0.21$ was computed from all the calibrated values. The two approaches for determining the values of $K^*$ were employed in the model verification and both gave equally good agreement with the experimental measurements.

Fig. 2(b) indicates that $K$ is more sensitive than $K^*$ to the variation in the junction angle especially for angles between 30° and 90°. The figure shows a generally linear increase in $K$ with the junction angle, with the exception of one data point. Thus, a second trend line was plotted for the variation of $K$ with $\delta$, again excluding the data of Gurram (1994). The equation of the trend line is

$$K = 0.0092\delta - 0.1855 \tag{20}$$

with a coefficient of determination of 0.91. Eq. (20) was used to compute the empirical values of $K$ for the angles considered in the subsequent analysis.

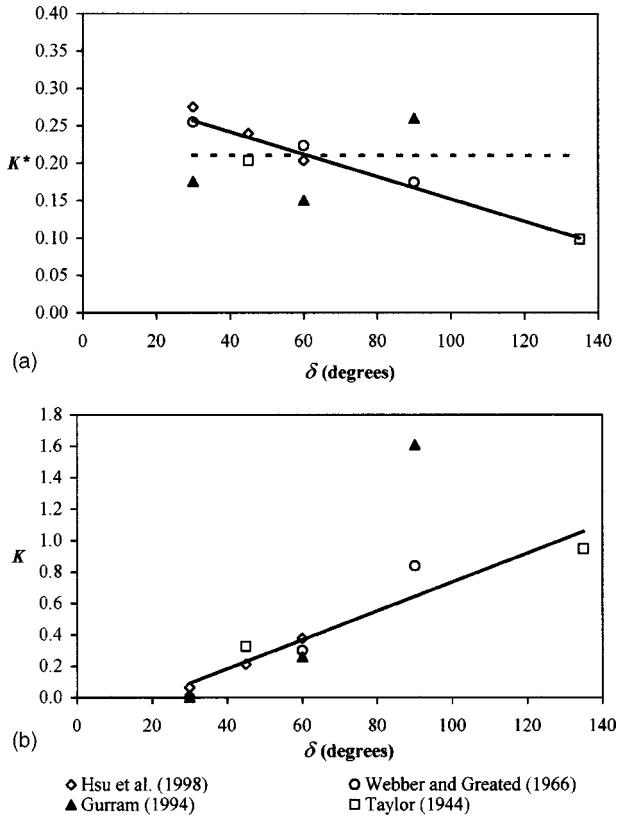


**Fig. 2.** (a) Variation of $K^*$ with junction angle and (b) variation of $K$ with junction angle

### Final Model Results

Figs. 3(a and b) present the variation of the measured and the computed depth ratios, $\eta_1$, and $\eta_2$, with $\xi$, for the three angles of intersection (30°, 45°, and 60°) that Hsu et al. (1998) investigated. The computations for the proposed momentum approach are presented for two cases: the first where the interfacial or separation shear forces are not included and the second where they are included. Eqs. (19) and (20) are used to estimate $K^*$ and $K$ for the second case. The figure shows a good agreement between the computations and the measurements. This indicates that $K^*$ and $K$ are independent of the discharge ratio.

Figs. 3(a and b) also present a comparison between the proposed momentum approach and two energy approaches: the common approach of the equality of the water surface elevations ($\eta_1 = \eta_2 = 1$) (neglecting velocity heads and losses); and the simple energy approach (conservation of energy while neglecting losses). The comparison shows that assuming all three water surface elevations are equal, represented by the x axis in Figs. 3(a and b), does not reflect the actual experimental observations. Including the velocity heads improves the predictions, but still underestimates both upstream depths for most discharge ratios.

The proposed momentum approach, without including the interfacial shear or the separation zone shear terms ($K^* = 0, K = 0$), shows an improvement in the predictions over the energy approaches for most discharge ratios. This indicates that the basic curvilinear two-control volume approach is valid and that a reasonable first approximation may be obtained without any calibration. Some discrepancy in both $\eta_1$ and $\eta_2$ is still evident but can be reduced by including the secondary force terms. The two shear terms in the analysis have a small effect at discharge ratios around 0.5. However, at the higher- and lower-discharge ratios these

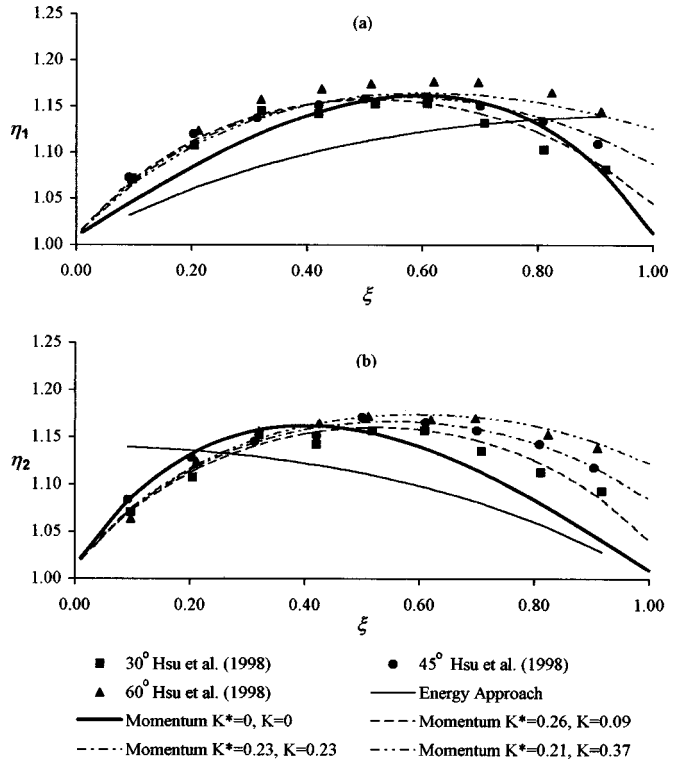


**Fig. 3.** Comparison of model predictions with Hsu et al. (1998): (a) main channel depth ratio $\eta_1$ and (b) lateral channel depth ratio $\eta_2$

terms have a more significant effect in that the interfacial shear tends to further equalize the depth ratios while the separation shear term captures the increased upstream depths with larger lateral channel discharges and angles.

Figs. 4(a–d) present plots of the computed depth ratios $\eta_1$ and $\eta_2$ against $F_3$. The calculated depth ratios are presented in each plot for two cases, the first not including the interfacial or the separation shear terms ($K^*=0, K=0$) and the second while including them. In the latter, the empirical values of both coefficients for each case were used in the calculations. The good agreement between the proposed model predictions and the measurements for the different angles indicate that the interfacial and separation coefficients are independent of the downstream Froude number.

The consistency of the model results with the observation of equal upstream depths ($\eta_1=\eta_2$) used as an assumption in previous theories may be verified by comparing the computed depth ratios while including the interfacial shear in each of the Figs. 4(a–d).

In practice, both $K^*$ and $K$ should be treated as calibration coefficients. In this study, these coefficients were found to be independent of the discharge ratios and the downstream Froude number but were dependent on geometry. For practical cases, once they have been calibrated for a specific geometry at known flow conditions, it may be possible to use the same values for different flow situations.

## Comparison with Previous Theories

Comparisons between the proposed momentum approach and the theories of Taylor (1944); Webber and Greated (1966); Gurram (1994); and Hsu et al. (1998) were performed. Webber and Greated (1966) presented a theory similar to Taylor's (1944) but in terms of the downstream Froude number instead of the kineticity coefficient. Fig. 5 presents the comparisons with Taylor's (1944); Webber and Greated (1966); and Gurram's (1994) theories. The figure also includes the available data for each angle and each discharge ratio. In this figure the graph's origin on the abscissa scale is shifted progressively to the right. The comparisons with the theory of Hsu et al. (1998) are presented in Figs. 6(a–b).

Fig. 5 presents the comparisons for the case of a constant junction angle of 60° and different discharge ratios (0.2, 0.25, 0.4, 0.5, 0.6, 0.75, and 0.8). For this angle, $K^*$ of 0.21 and $K$ of 0.37 represent both the mean and the empirical values. Webber and Greated's (1966) and Gurram's (1994) experimental data are

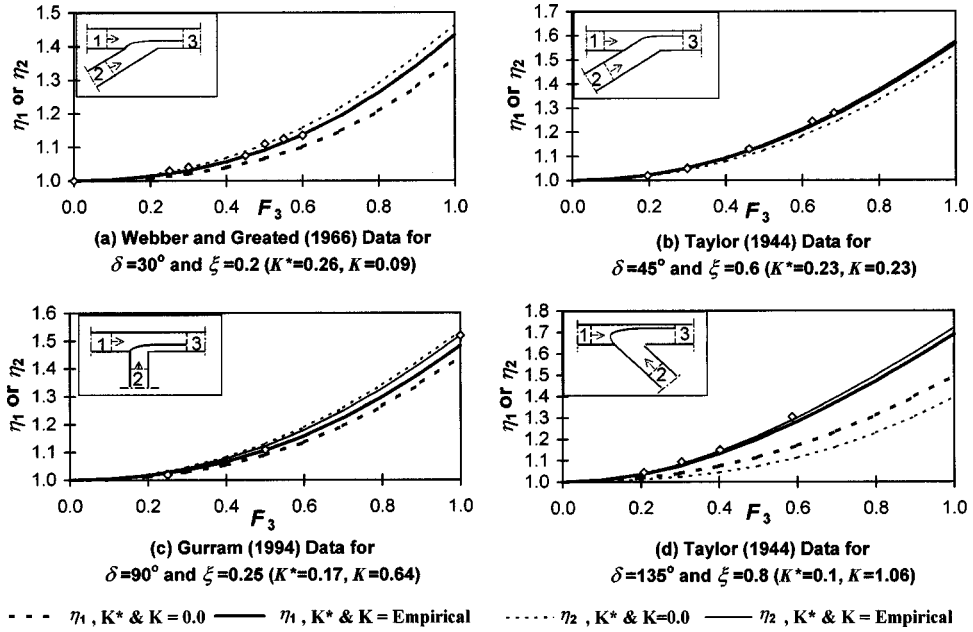


**Fig. 4.** Final model equations' results

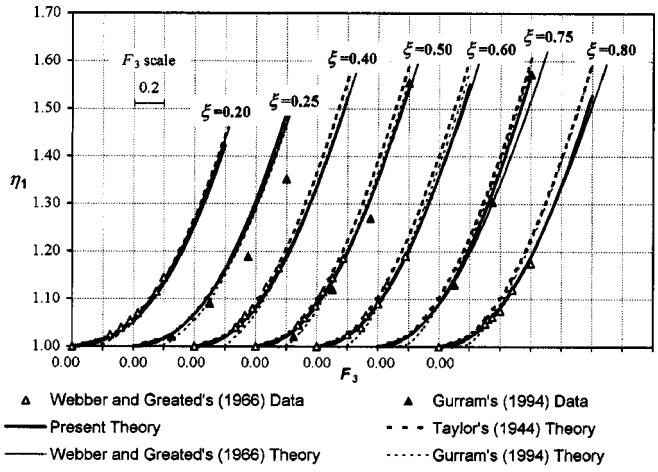


**Fig. 5.** Comparing different theories ($\delta = 60°, K^* = 0.21, K = 0.37$)

shown for validation. Figs. 6(a–b) present the case of a constant downstream Froude number $F_3 = 0.53$ and different discharge ratios.

On comparing the model equations with the different theories it can be seen that the model predictions for both depth ratios are generally as good as the other theories for most discharge ratios and slightly superior for high-discharge ratios. The advantage of the proposed approach over these other theories is in its capability to be scaled up to prototype applications, since it includes most of the physical effects neglected in other theories. The boundary friction force has been neglected in all of the other theories and although this works well at model scales, it is significant in real-world cases. For example, consider two cases: the first, a real river with an aspect ratio of 100 and a Chezy $C_*$ of 10 and the second, an experimental flume with an aspect ratio of 3 and a Chezy $C_*$ of 17. Keeping the discharge ratio, the width ratios, and the downstream Froude number the same and performing an order of magnitude analysis for the different terms in Eqs. (17) and (18) in both cases, we find that in the first case the friction term is almost of the same magnitude as the net pressure term. However, in the second case the friction term is negligible. The second advantage of the proposed model is that it does not rely on the assumption of equality of the upstream depths in both the main and the lateral channels. For general situations, this assumption may not be applicable.

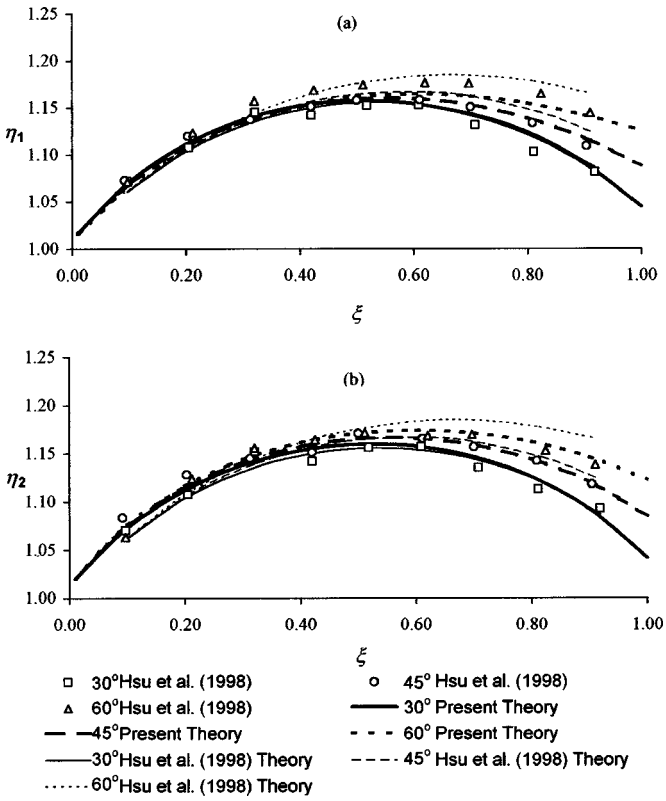


**Fig. 6.** Comparison with theory of Hsu et al. (1998): (a) main channel depth ratio $\eta_1$ and (b) lateral channel depth ratio $\eta_2$

## Summary and Conclusions

A one-dimensional theoretical model providing the necessary interior boundary equations governing combining subcritical open channel junctions was developed. The momentum principle was applied to two control volumes in the junction, in the respective streamwise directions. Given the inflow discharges and a downstream boundary condition, the model calculates the upstream depths for each of the incoming channels.

The interfacial shear force between the two control volumes and the separation zone shear force in the lateral channel control volume were included in the analysis. Two shear coefficients were calibrated, using the available experimental data, for the different junction angles. It was found that the variation in these coefficients was independent of the discharge ratio and the downstream Froude number but was dependent on the angle of intersection. From this we tentatively conclude that, in general, the coefficients are dependent on junction geometry, but not on flow. The latter conclusion requires further experimental verification, but may be acceptable as a working hypothesis in practical cases.

A comparison between the current treatment for junctions in open channel network models that apply conservation of energy and the proposed model was performed. It was found that the basic momentum formulation, neglecting shear forces, gave an approximation for the upstream depths which was superior to the energy approach with no losses.

A comparison between the proposed theory, including shear forces, and previous momentum-based theoretical approaches was performed. The comparison showed that the proposed model predictions were about as good as the other theories and somewhat superior at high-discharge ratios. The advantage of the proposed theory is that it models almost all of the physical effects involved, such as the boundary friction forces which were neglected in all of the other theories, and thus it can be scaled up to real-world applications. Further, the application of the momentum principle in the streamwise direction to two control volumes in the junction allows the model to be easily implemented in network models and makes handling of the junctions consistent with that of the channel reaches.

With the addition of terms for storage of mass and momentum, the present model could be readily extended to an unsteady dynamic junction model. The two junction control volumes could be treated as regular channel cells, including storage of mass and momentum terms, albeit with consideration of variable width and extra interaction terms. Unfortunately, no experimental data is available at this time for verification of such a model.

## Acknowledgments

This research was funded through grants and scholarships from the Natural Sciences and Engineering Research Council of

Canada as well as by a Province of Alberta Fellowship. The writers would also like to thank Willi H. Hager, K. S. Karki, S. Kumar Gurram, and Chung-Chieh Hsu for sending their experimental data.

## Notation

*The following symbols are used in this paper:*

$A$ = cross-sectional area;
$B$ = pressure force due to change in control volume width;
$b$ = channel width;
$C_f$ = coefficient of friction;
$C_*$ = Chezy coefficient;
$\mathsf{F}$ = Froude number;
$\mathsf{F}_b$ = frictional shear force;
$\mathsf{F}_s$ = separation zone shear force;
$g$ = gravitational acceleration;
$K$ = separation zone shear coefficient;
$K^*$ = coefficient of interfacial shear;
$L$ = length of control volume;
$L_i$ = length of interface between two control volumes;
$L_s$ = length of separation zone interface;
$P$ = hydrostatic pressure force;
$Q$ = discharge;
$\mathsf{R}$ = Reynolds number;
$S$ = shear force on interface;
$V$ = mean velocity;
$W$ = weight of water in control volume;
$y$ = depth;
$\delta$ = lateral angle;
$\gamma$ = specific weight of liquid;
$\eta$ = depth ratio;
$\xi$ = discharge ratio;
$\rho$ = density of liquid; and
$\omega$ = width ratio.

**Subscripts**

$^1$ = main channel section for section parameters ($A$, $b$, $\mathsf{F}$, $P$, $Q$, $\mathsf{R}$, $y$, $V$), main channel control volume for control volume parameters ($B$, $\mathsf{F}_b$, $\mathsf{F}_s$, $L$, $\eta$, $\omega$);
$^2$ = lateral channel section for section parameters ($A$, $b$, $\mathsf{F}$, P, Q, $\mathsf{R}$, $y$, $V$), lateral channel control volume for control volume parameters ($B$, $\mathsf{F}_b$, $\mathsf{F}_s$, $L$, $\eta$, $\omega$); and
$^3$ = downstream channel section.

## References

Best, J. L., and Reid, I. (1984). "Separation zone at open-channel junctions." *J. Hydraul. Eng.*, 110(11), 1588–1594.

Chaudhry, M. H. (1993). *Open-channel flow*, Prentice-Hall, Englewood Cliffs, N. J.

Danish Hydraulic Institute. (1999). Denmark ⟨http://www.dhi.dk⟩.

Environment Canada, Water Modeling Section. (1988). "One dimensional hydrodynamic model." Water Planning and Management Branch, Environment Canada.

Garcia-Navarro, M. P., and Savirón, J. M. (1992). "Numerical simulation of unsteady flow at open channel junctions." *J Hydraul. Res.*, 30(5), 595–609.

Gurram, K. S. (1994). "A study of subcritical and transitional combining flow in open channel junctions." PhD thesis, Banaras Hindu Univ., Varanasi, India.

Hsu, C.-C., Lee, W.-J., and Chang, C.-H. (1998). "Subcritical open channel junction flow." *J. Hydraul. Eng.*, 124(8), 847–855.

Rajaratnam, N. (1976). *Turbulent jets*, Elsevier, The Netherlands, 304.

Taylor, E. H. (1944). "Flow characteristics at rectangular open channel junctions." *Trans., Am. Soc. Civ. Eng.*, 109, 893–912.

Webber, N. B., and Greated, C. A. (1966). "An investigation of flow behavior at the junction of rectangular channels." *Proc., Institute Civil Engineers*, Vol. 34, London, 321–334.